Journal of Membrane Science 653 (2022) 120556

Contents lists available at ScienceDirect

Journal of Membrane Science

journal homepage: www.elsevier.com/locate/memsci

Time-resolved pressure-induced electric potential in nanoporous membranes: Measurement and mechanistic interpretation

Pavel Apel [a], Stanisław Koter [b,*], Andriy Yaroshchuk [c,d,**]

[a] Joint Institute for Nuclear Research, Joliot-Curie str. 6, 141980, Dubna, Russian Federation
[b] Faculty of Chemistry, Nicolaus Copernicus University in Toruń, Gagarin St. 7, 87-100, Toruń, Poland
[c] ICREA, pg. L.Companys 23, 08010, Barcelona, Spain
[d] Department of Chemical Engineering, Universitat Politècnica de Catalunya, av. Diagonal 647, 08028, Barcelona, Spain

ARTICLE INFO

Keywords:
Pressure-induced potential
Streaming potential
Time-resolved measurements
Nanoporous membrane
Surface charge
Theoretical model

ABSTRACT

Performance of charged nanoporous membranes in ion separations and electrokinetic energy conversion is controlled by their surface-charge density. This (or related such as zeta-potential) parameter has often been obtained from measurements of pressure-induced electric potential typically referred to as streaming potential. However, with nanoporous membranes in dilute electrolyte solutions, determination of genuine streaming potential is non-trivial and requires time-resolved measurements. A new approach to the interpretation of such measurements developed and tested experimentally in this study makes possible parallel determination of several membrane transport properties while previously only streaming-potential coefficient was determined. In nanoporous membranes, this coefficient is a non-monotone function of surface-charge density, which makes difficult unambiguous determination of the latter. On the contrary, the other properties determined in this study are monotone functions of surface-charge density. This approach has been validated via characterization of two nanoporous track-etched membranes (with the pore sizes of 25 nm and 35 nm) in KCl solutions and revealed an excellent applicability. The transport properties "extracted" from experimental data were used as input of full (numerical) version of space-charge model. This made possible determination of surface-charge density as well as some properties of hypothetical gel layers reportedly surrounding pores of nanoporous grades of track-etched membranes.

1. Introduction

Charged nanoporous membranes show an interesting ion-separation behavior controlled by fixed electrical charges on their pore surface [1–3]. They also feature rather high efficiencies in electrokinetic energy conversion [4–6]. Therefore, quantitative characterization of their electrochemical properties is of interest. Transversal streaming potential has often been used as a tool for characterization of various membranes. If the membrane pores are sufficiently large compared to the thickness of diffuse parts of Electric Double Layers (EDL) (Debye screening length) the measurement and its interpretation are relatively simple and straightforward. Thus for instance, Ref. [7] investigated a microporous inorganic membrane (average pore size 0.9 μm) with solutions of >1 mM concentration. Due to the large pore size (relative to the screening length of <10 nm) salt rejection was negligible and true streaming potential could be measured. Weak EDL overlap also occurred (owing to the use of relatively concentrated solutions with ionic strength of 50 mM) in much smaller pores (40–60 nm) studied in Ref. [8]. Because of this, salt rejection was also negligible and measurements of steady-state pressure-induced potential yielded streaming-potential coefficient. The smallest pore size of track-etched membranes investigated in Ref. [9] was around 20 nm while the KCl concentration was 10 mM (screening length 3 nm). This likely made the salt rejection quite low and the measurements of stationary filtration potential suitable for the determination of streaming-potential coefficient.

However, once the pore size becomes commeasurable with the screening length (and the pore surface has fixed charges) application of *trans*-membrane pressure gives rise to a more or less pronounced salt rejection. This causes time dependent salt-concentration gradients (both inside and outside the membrane) and coupled diffusion potentials. As a

* Corresponding author.
** Corresponding author.ICREA, pg. L.Companys 23, 08010, Barcelona, Spain.
E-mail address: skoter@umk.pl (S. Koter).

https://doi.org/10.1016/j.memsci.2022.120556
Received 5 February 2022; Received in revised form 6 April 2022; Accepted 7 April 2022
Available online 11 April 2022

result, pressure-induced potential difference also becomes time-dependent, and determination of genuine streaming potential requires special procedures. Their further development is one of the objectives of this study. Additionally, for the first time we will use the slope of initially linear dependence of diffusion-related voltage on square root of time as well as characteristic relaxation time fitted to experimental data for the interpretation.

In the literature, these phenomena have often been overlooked. Thus for instance, Ref. [10] reported on the measurements of "streaming" potential across polycarbonate track-etched membranes (some of them having pores of 10 nm, 15 nm and 30 nm diameters) in dilute (1 mM KCl) solutions. The data were taken after prolonged signal-stabilization periods. Given that membranes with quite small pores were used, considerable salt rejections probably occurred, so the signal could have significant diffusion-potential components. Their relative contribution decreased with increasing membrane pore size, which might have influenced some of the conclusions made in Ref. [10] concerning correlations of apparent zeta-potential with the pore size. Stationary pressure-induced (referred to as "streaming") potential was also studied in Ref. [11] using a 4-nm pore-size inorganic membrane in electrolyte solutions of various concentrations including very dilute ones (0.5 mM). Given that salt rejections were also directly measured in parallel, the measured *trans*-membrane potentials clearly had diffusion-related components. Similar approach was used by Condom et al. [12] while time stabilization needed to reach stationary *trans*-membrane potential difference was explicitly mentioned. Measurements of pressure-induced potential (after a 1-min stabilization) were also performed in Ref. [13] for various nano-engineered "membranes" having identical slit-like nanopores (from 2.5 nm to 50 nm in height) in pH-buffered 10 mM KCl solutions. According to our analysis below, with the smaller pore sizes the measurements could be noticeably affected by salt rejection and associated diffusion potential. However, no information on the time dependence is provided. Moreover, there is also no information on the membrane porosity, which makes impossible estimates of characteristic relaxation time according to Eq (14) below. Nevertheless, we will see that considerable build-up of diffusion potential occurs already at times much shorter than the characteristic relaxation time. Therefore, it is highly likely that the measurements reported in Ref. [13] were affected by concentration polarization and, thus, did not correspond to genuine streaming potential. Ref. [14] studied pressure-induced potential with a series of track-etched membranes in a broad concentration range (from 0.01 mM to 10 mM) in LiCl solutions. For the membranes with the smallest pore size (134 nm) in most dilute solutions, salt rejection could make the *trans*-membrane potential time-dependent but no information on this is provided. No information on the time dependence of pressure-induced potential is provided in Ref. [15], either. Meanwhile, salt rejections were directly measured with the same membranes and under the same conditions as the "streaming" potentials, so concentration polarization certainly occurred and had to give rise to time dependencies. Ref. [16] reported on the measurements of "streaming" potential with a composite ceramic membrane having average pore size of 27 nm for a broad range of KCl concentrations (from 0.2 mM to 1 M). The pressure difference was reportedly applied in "pulses" but their duration was not specified. Given the hydraulics of the cross-flow cell used in Ref. [16], it is unlikely that the pulses could be very short. Accordingly, the measurements in more dilute solutions were likely affected by an uncontrolled buildup of *trans*-membrane concentration difference. Pressure-induced transmembrane potential was also studied in Ref. [17] using a 5-nm cobalt-spinel ceramic membranes. Due to the membrane rigidity, the measurements could be performed up to rather high pressures (1.2 MPa) without noticeable changes in the membrane structure. This afforded determination of streaming potential from the slope of linear part of pressure dependence occurring at higher pressures (while the lower-pressure part was non-linear due to the buildup of concentration polarization). However, time-resolved measurements (that could provide additional input) were not performed. Ref. [18] pointed out that pressure-induced potential difference across RO membranes included components other than streaming potential due to salt rejection. However, no time-resolved measurements were performed to single out various components.

Zhang and Xu [19] studied pressure-induced potential with a series of lab-made anion-exchange membranes in various electrolyte solutions. While studying dependencies on the direction of variation of applied pressure (stepwise decreasing vs. increasing) they observed considerable hysteresis, which they correctly ascribed to salt-rejection phenomena. In fact, this approach exploited time dependencies in a sense. However, additional opportunities offered by explicit time-resolved measurements were not explored. Non-linear and time-resolved (after pressure switch-off) measurements were combined in Ref. [20] (using a nanoporous track-etched membrane). This made possible a consistent interpretation within the scope of space-charge model. However, ref. [20] used a sophisticated stirred test cell enabling pressure switch-offs within as short as 5–10 ms (from pressures as high as 0.6 MPa needed to observe a pronounced linear part at higher pressures). In the present study, we will use a much simpler experimental setup. Ref. [21] performed time-resolved measurements of pressure-induced potential with a poly-methacrylic-acid grafted polyethylene membranes and developed an empirical model for their interpretation. The model postulated existence of a membrane-associated "capacitor" that was gradually charged after application of pressure. The physical meaning of this capacitor was not explained. Time-resolved measurements of *trans*-membrane potential were also carried out in Ref. [22]. However, in this study the time dependence was due to gradually changing *trans*-membrane pressure difference while a wide porous track-etched membrane (0.8 μm) without salt rejection was used.

The approach used in the present study was proposed and initially developed in Refs. [23,24]. The model developed in Ref. [23] for an ion-exchange membrane postulated zero salt flux through the membrane. This model was transferred without modification to the case of track-etched membranes studied in Ref. [24]. To obtain streaming-potential coefficient, these studies used only extrapolated (to very short times) values of pressure-induced potential. Therefore, this approximation did not affect the validity of their conclusions. In the present study, we will go beyond the short-time extrapolation and use the whole signal time dependence for the interpretation. We will also allow for a transmembrane salt flux in the model. This will afford obtaining two additional experimental parameters: initial slope of dependence of pressure-induced potential on square root of time, and characteristic relaxation time. Availability of this additional input will make possible detailed quantitative comparison with the space-charge model of ion distribution inside nanopores and checks of self-consistency of this interpretation. Quantitative interpretation will be additionally favored by the use in experiments of nanoporous track-etched membranes with a well-defined cylindrical pore geometry. Remarkably, just this kind of membranes has been demonstrated to be very effective in strong separations of ions of equal charge but different mobilities (K^+/Li^+) [1]. High selectivities could be achieved due to the very narrow pore size distribution. Besides, the noticeable thickness of these membrane (compared to the typical thicknesses of active layers of composite/asymmetric membranes) in combination with the pore size in the range of single tens of nanometers made possible achieving the mode of large Péclet numbers (at a relatively weak concentration polarization), which is instrumental for the high selectivities. No other type of membranes at present possess this combination of properties.

Theoretical framework of space-charge model was laid down in Refs. [25,26] and further developed in Refs. [13,27–31]. As pointed out by Refs. [13,32], in nanopores streaming-potential coefficient (proportional to the so-called apparent zeta-potential) is a non-monotone function of surface potential (surface charge density). The present study will demonstrate that both additional input parameters (initial slope and characteristic relaxation time) depend on the surface-charge density in monotone way. This will make possible unambiguous

determination of the latter.

2. Theory

2.1. Model of pressure-induced non-stationary salt rejection and diffusion

This study considers conditions of zero electric current, so the fluxes of ions are stoichiometric, and one can consider only time-dependent salt diffusion. In media with ion perm-selectivity, salt-concentration gradients are known to give rise to voltage gradients (arising to make the ion flows stoichiometric). The corresponding voltage differences will be measured in experiments where we use relatively low pressures. Therefore, concentration differences across the membrane are small. The validity of these approximations will be checked a posteriori using experimental data.

At times much longer than the characteristic time of diffusion relaxation over the membrane thickness, L, (given that $L \approx 10\ \mu m$, $L^2/D_m \approx 0.05\ s$ (D_m is the salt diffusion coefficient in membrane pores) for the membranes and solutions used in this study) insides the membrane salt-concentration profile is practically linear and the salt flux is position-independent (but depends on time). Salt concentration increases at the feed membrane surface because a part of salt is rejected by the membrane. Simultaneously, at the permeate side, salt concentration decreases (due to partial dilution) because the solvent is transferred through the membrane better than the salt. In the linear approximation of small transmembrane concentration differences, the corresponding changes of concentration at the membrane surfaces are equal in magnitude and opposite in sign as illustrated in Fig. 1.

Taking additionally into account that the salt-concentration profile inside the membrane is linear, we see that the problem can be formulated for only one half of the membrane while solution in the other half can be obtained from the anti-symmetry considerations. The transmembrane salt flux is a combination of diffusion and advection

$$J_m(t) = 2P_m \Delta c(t) + J_v(t)(1-\sigma_s)c_0 \tag{1}$$

where P_m (m/s) is the diffusion permeance (permeability divided by thickness) of the membrane (the factor 2 arises because we consider only half of the membrane), $\Delta c(t) \equiv c(0,t) - c_0$ is the concentration difference between the feed surface of the membrane and its middle (due to the problem anti-symmetry, the concentration in the middle stays constant and equal to the equilibrium concentration, c_0), $J_v(t)$ (m/s) is the time-dependent *trans*-membrane volume flux, σ_s (dimensionless) is the salt reflection coefficient, $x = 0$ at the feed membrane surface (the side where the volume flow is "entering" the membrane).

Outside the membrane, we have this standard non-stationary convection-diffusion equation:

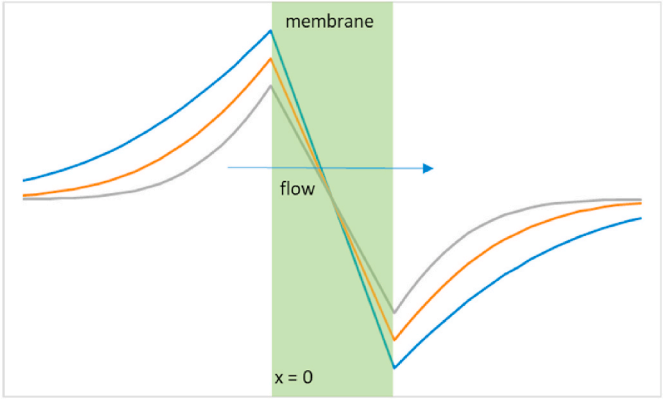

Fig. 1. Schematic of time-dependent profiles of salt-concentration deviation from equilibrium value (various dimensionless times: $\tau = 0.25; 0.5; 1$).

$$\frac{\partial c}{\partial t} = D\frac{\partial^2 c}{\partial x^2} - J_v(t)\frac{\partial c}{\partial x} \tag{2}$$

where D (m^2/s) is the salt diffusion coefficient in the solution, and this expression for the salt flux

$$J(x,t) = -D\frac{\partial c}{\partial x} + J_v(t)c \tag{3}$$

Taking into accounts Eq (1), the boundary condition to Eq (2) for the salt flux at the feed membrane surface is

$$J(0,t) = 2P_m(c(0,t) - c_0) + J_v(t)(1-\sigma_s)c_0 \tag{4}$$

The other boundary condition reflects the fact that concentration changes never reach very far away from the membrane

$$c(-\infty, t) = c_0 \tag{5}$$

Prior to the start of the measurement, the system is in equilibrium, transmembrane volume flux is zero, and salt concentration is constant everywhere. Accordingly, the initial condition is

$$c(x,0) = c_0 \tag{6}$$

For the dimensionless deviation of concentration from equilibrium value

$$s(x,t) \equiv \frac{c(x,t)}{c_0} - 1 \tag{7}$$

From Eqs(3) and (4), we obtain

$$-\frac{D}{2P_m}\frac{\partial s(0,t)}{\partial x} + Pe(t)s(0,t) = s(0,t) - Pe(t)\sigma_s \tag{8}$$

where we have denoted

$$Pe(t) \equiv J_v(t)/2P_m \tag{9}$$

Due to the assumed low volume fluxes

$$Pe(t) \ll 1 \tag{10}$$

The dimensionless concentration deviation is proportional to $Pe(t)$ and is also small, so the term $Pe(t)s(0,t)$ is of the second order and can be neglected, and Eq (8) transforms to

$$\frac{\partial s(0,t)}{\partial \xi} + s(0,t) = Pe(t)\sigma_s \tag{11}$$

where we have introduced dimensionless coordinate, ξ, according to

$$\xi \equiv x \cdot \frac{2P_m}{D} \tag{12}$$

Equation for the non-stationary salt convection-diffusion outside the membrane (Eq (2)) can also be reformulated in terms of dimensionless concentration deviation, dimensionless coordinate and dimensionless time defined by

$$\tau \equiv t/t_{ch} \tag{13}$$

$$t_{ch} \equiv D/4P_m^2 \tag{14}$$

Additionally taking into account that $Pe(t)\frac{\partial s}{\partial \xi}$ is of the second order, we obtain

$$\frac{\partial s}{\partial \tau} = \frac{\partial^2 s}{\partial \xi^2} \tag{15}$$

If the flux is increased step-wise

$$Pe(t) = Pe_0 H(\tau) \tag{16}$$

where $H(\tau)$ is the unit-step (Heaviside) function. In the approximation of small fluxes, in dimensionless variables the boundary and initial con-

ditions can be summarized this way

$$\frac{\partial s(0,\tau)}{\partial \xi} + s(0,\tau) = Pe_0 \cdot \sigma_s \cdot H(\tau) \tag{17}$$

$$s(-\infty,\tau) = 0 \tag{18}$$

$$s(\xi,0) = 0 \tag{19}$$

Eqs (15), (17)–(19) are a standard linear non-stationary-diffusion boundary-value problem that can be solved by Fourier-transform method. The solution is sought in this form

$$s(\xi,\tau) \equiv \frac{1}{2\pi}\int_{-\infty}^{+\infty} d\omega exp(i\omega\tau) s(\xi,\omega) \tag{20}$$

By substituting Eq (20) to Eq (15), and taking into account the boundary condition of Eq (18), for the Fourier-transform of dimensionless deviation of concentration, we obtain

$$s(\xi,\omega) = A(\omega)\cdot exp\left(\sqrt{i\omega}\,\xi\right) \tag{21}$$

By using another boundary condition (Eq (17)), for the frequency-dependent coefficient, we obtain

$$A(\omega) = Pe_0\cdot\sigma_s\cdot\frac{H(\omega)}{1+\sqrt{i\omega}} \tag{22}$$

where $H(\omega)$ is the Fourier-transform of unit-step function

$$H(\omega) \equiv \pi\delta(\omega) - \frac{i}{\omega} \tag{23}$$

Substituting Eqs (22) and (23) to Eq (20), we obtain

$$s(0,\tau) \equiv A(\tau) \equiv Pe_0\sigma_s\left[1 - \frac{1}{2\pi}Re\left(\int_{-\infty}^{+\infty} d\omega \frac{exp(i\omega\tau)}{\sqrt{i\omega}\left(1+\sqrt{i\omega}\right)}\right)\right] \quad \tau \geq 0 \tag{24}$$

The integral can be taken in terms of MeijerG special function, which is available, for example, in Maple 2020 software. Besides, as the integral depends only on dimensionless time it can be tabulated just once. A polynomial approximation is provided in the Electronic Supporting Information (ESI).

An approximate analysis of a similar problem (at short dimensionless times) was carried out in Ref. [23] where the bracketed term in the right-hand side of Eq (24) was shown to be approximately equal to

$$1 - \frac{1}{2\pi}\int_{-\infty}^{+\infty} d\omega \frac{exp(i\omega\tau)}{\sqrt{i\omega}\left(1+\sqrt{i\omega}\right)} \approx 2\sqrt{\frac{\tau}{\pi}} - \tau \quad (\tau \ll 1) \tag{25}$$

Eqs 24 and 25 show that the initial part of dependence of dimensionless deviation of concentration (and the diffusion-related voltage component proportional to it, see Eq (28) below) on square root of time should be linear. This is confirmed by Fig. 2 showing the bracketed term in Eq (24) as a function of square root of dimensionless time.

The initial linearity of dependence on square root of time was exploited in Refs. [23,24] to extrapolate pressure-induced potential measured after stepwise application of pressure to zero time and, thus, obtain genuine streaming potential.

2.2. Limitations of the model

Fig. 2 shows that the dependence can reasonably be considered linear only at $\tau \leq 0.1$. At longer dimensionless times, it becomes sublinear (which is partially captured by the second term in the right-hand side of Eq (25)) and slowly tends to one at very long dimensionless times (not shown in Fig. 2, see Fig. S1 in the ESI). Therefore, according to Eq (24) stationary salt rejection (equal to double dimensionless concentration deviation at the membrane surface, see Fig. 1) increases linearly with Péclet number while in reality it should go to saturation. This linear increase is a consequence of the use of linear approximation in the dimensionless deviation of salt concentration. Below, we will verify a posteriori that Péclet number was really small in our experiments.

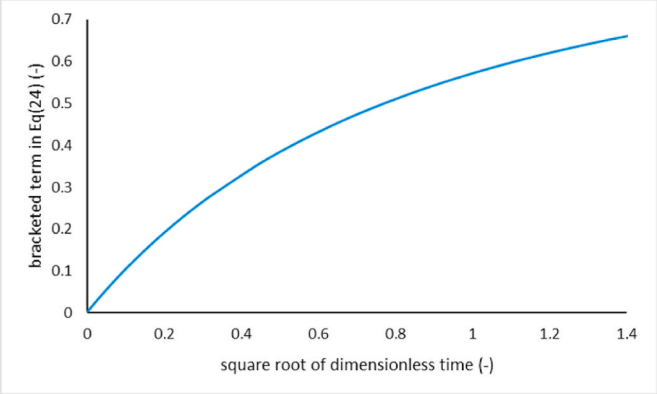

Fig. 2. Time dependence in Eq (24).

Another limitation of our model is related to the assumption of stagnant solutions. In reality, there is always some natural convection, which effectively imposes initial salt concentration not at infinity but at a finite distance from the membrane surface. The magnitude of this distance is still a matter of debate [33,34]. Some authors have argued that (in water) it may be around 500 μm [33]. Once the spatial range of concentration perturbation starts approaching the "natural-convection-controlled" stagnant-layer thickness, our model begins to overestimate the concentration-difference buildup. Assuming a 500-μm stagnant layer, the time of diffusion-front propagation over such distance ($\sim \delta^2/D$) can be estimated as approximately 100 s (in KCl solutions used in our experiments). At shorter times, our model of stagnant solutions should be applicable. Given the uncertainty with the value of "natural-convection-controlled" stagnant-layer thickness, we limited the "exploitable" (used for interpretation) duration of our measurements to ca.40 s.

Our simple analytical model also neglects the build-up of osmotic pressure (the volume flux is assumed to stay constant after the hydrostatic-pressure step). This limits its applicability to rather dilute solutions, relatively small salt-reflection coefficients and/or sufficiently short elapsed times when a considerable buildup could not occur, yet. The transmembrane osmotic-pressure difference is proportional to the concentration difference between the feed and permeate sides of the membrane and to the salt reflection coefficient. As we can see from Eq (24), the concentration difference is proportional to the salt-reflection coefficient, too. Taking all this into account, the ratio of maximum osmotic-pressure (occurring at very long times) to the "driving" hydrostatic-pressure difference is approximately given by this

$$\frac{4Pe_0\sigma_s^2 RTc_0}{\Delta p} \approx 2RTc_0\frac{\sigma_s^2\chi_*}{P_m} \tag{26}$$

From Fig. 2, we see that within a unit dimensionless time (a typical duration of our measurements) about 50% of stationary salt-concentration difference already builds up. Accounting for this (and using the values of salt-reflection coefficient, diffusion and hydraulic permeabilities fitted to the experimental data, see below) a posteriori estimates show (see the ESI) that osmotic-pressure differences could amount to 1.3%–2.5% of the applied hydrostatic-pressure differences by the end of a typical single measurement. As a result, the signal increase could be slightly slowed down, which might result in somewhat underestimated characteristic relaxation times but these corrections are minor.

2.3. Electrical response to concentration gradients

As we can see from Fig. 1, there are three zones with concentration gradients in the system: two zones outside the membrane and one inside it. Electrical response to a concentration gradient under zero-current conditions is known to be controlled by ion transport numbers and (in the case of (1:1) electrolytes used in our experiments) can be expressed this way [20,35,36].

$$\nabla\varphi = \frac{RT}{F}(t_+ - t_-)\nabla ln(c) \equiv \frac{RT}{F}(2t_+ - 1)\frac{\nabla c}{c} \tag{27}$$

Outside the membrane, the ion transport numbers are controlled by bulk ion mobilities. Inside the membrane, there is an additional difference between them due to electrostatic interactions between ions and surface charges giving rise to enhanced concentration of counterions and reduced concentration of coions. Since the salt concentrations in two reservoirs are equal, the sum of concentration differences across the two diffusion layers is equal in magnitude and opposite in sign to the concentration difference across the membrane, so the sum of all concentration differences in the system is zero. Nevertheless, due to the different ion transport numbers in the membrane and solution, a net electrical response to such situation is non-zero. Assuming that (due to the small deviations of concentration from the equilibrium value) ion transport numbers inside the membrane are independent of concentration (outside the membrane they are reasonably constant anyway), we can integrate Eq (27) within each zone and add up the corresponding voltage differences (with the due account of their signs). As a result, for the full diffusion-related voltage difference across the system (measurable with a pair of reversible electrodes located outside the concentration-polarization layers), we obtain

$$\Delta\varphi_d(\tau) = \frac{4RT}{F}\left(t_+^{(m)} - t_+^{(b)}\right)s(0,\tau) \tag{28}$$

where $t_+^{(m)}, t_+^{(b)}$ are the cation transport numbers in the membrane and solution bulk, respectively. While deriving Eq (28), we took into account that $s(0,\tau)$ is the half of the relative concentration difference across the membrane (see Fig. 1). In addition to this diffusion-related response, there is an instantaneous response due to the advective movement of charged liquid through the pores. This is a true streaming potential.

According to Eq (25), the slope of the initially linear dependence of $s(0,t)$ on the square root of dimensionless time is $2Pe_0\sigma_s/\sqrt{\pi}$. Therefore, for the initial slope of dependence of voltage difference on dimensional time (directly obtainable from experiment) we get (taking into account the definitions of Péclet number, Eq (9), and characteristic relaxation time, Eq (14))

$$\frac{RT}{F}\frac{8}{\sqrt{\pi}}\sigma_s\left(t_+^{(m)} - t_+^{(b)}\right)\frac{J_{v0}}{\sqrt{D}} \approx \frac{RT}{F}\frac{8}{\sqrt{\pi}}\sigma_s\left(t_+^{(m)} - t_+^{(b)}\right)\frac{\chi_*}{\sqrt{D}}\frac{\Delta p}{L} \tag{29}$$

where χ_* ($m/s{\cdot}Pa$) is the membrane hydraulic permeability at zero current, L (m) is the membrane thickness, J_{v0} (m/s) is the transmembrane volume flow, Δp (Pa) is the *trans*-membrane pressure difference. While transforming from the left-to the right-hand side of Eq (29), we neglected the reduction of transmembrane volume flow due to the buildup of osmotic pressure difference (see above and the ESI for a posteriori estimates of this minor correction).

Given that the membrane hydraulic permeance, χ_*/L, is measurable independently, and bulk salt diffusion coefficient is known, from the initial slope of time-dependent voltage component (streaming-potential component arises instantaneously) one can determine the product of salt reflection coefficient and difference of cation transport numbers between the membrane and solution. By assuming that the pore size can be determined from the measured hydraulic permeability, known number of pores per unit area (track density) and membrane thickness, this parameter combination can be calculated (as a function of surface-charge density) using space-charge model outlined below. For membranes whose pores are much larger than hydrated-ion sizes, both salt rejection and increased counterion transport number occur due to electrostatic interactions of ions with pore-surface charges. Therefore, one can assume that both these parameters (and all the more so their product) would increase with the surface-charge density. Actually, for the salt-reflection coefficient, this is not always the case when the counterion diffusion coefficient is lower than that of coions [37]. However, in KCl solutions (with practically equal diffusion coefficients of cations and anions), the dependence on the surface-charge density is monotone. At the same time, it is known that in nanopores, streaming-potential coefficient is a non-monotone function of surface-charge density [13,32]. Moreover, below we will see that just for the pore sizes and salt concentrations used in this study, experimental values turn out rather close to the maxima of theoretical dependencies of streaming-potential coefficient on surface-charge density. This makes the monotone dependence of $\sigma_s(t_+^{(m)} - t_+^{(b)})$ on this parameter especially useful.

2.4. Space-charge model

For the mechanistic interpretation of membrane transport properties obtained from the time-transients, we will use full (numerical) version of space-charge model [31,38]. The corresponding derivations have been published elsewhere [39]. Here we will just reproduce (for the particular case of (1:1) salts) the expressions we are going to use.

Salt reflection coefficient:

$$\sigma_s \equiv 1 - (\tau_1 t_2 + \tau_2 t_1) \tag{30}$$

where τ_i are the so-called ion transmission coefficients (defined below by Eq (39)), the subscripts "1" and "2" denote two different ions of a binary electrolyte.

$$t_1 \equiv \frac{P_1 - \theta}{P_1 + P_2 - 2\theta} \tag{31}$$

Is the transport number of ion "1" at zero transmembrane volume flow, $t_2 \equiv 1 - t_1$, P_i are the ion permeabilities at zero volume flow, θ is the coefficient of "mutual electro-diffusion" at zero volume flow, namely, proportionality coefficient between the flux of one of the ions and the negative gradient of electrochemical potential of another ion.

Salt diffusion permeability at zero transmembrane volume flow is defined by

$$P_s \equiv \frac{2\left(P_1P_2 - \theta^2\right)}{P_1 + P_2 - 2\theta} \tag{32}$$

The membrane salt-diffusion permeance is $P_m \equiv P_s/L$.

Streaming-potential coefficient is defined by

$$\alpha \equiv \frac{RT}{F}\chi_*\frac{\tau_1 - \tau_2}{P_1 + P_2 - 2\theta} \tag{33}$$

where χ_* is the membrane hydraulic permeability at zero current defined by

$$\chi_* \equiv \frac{\chi}{1 + \chi\cdot\frac{\rho_{ek}^2}{g}} \tag{34}$$

$$\rho_{ek} \equiv Fc(\tau_1 - \tau_2) \tag{35}$$

Is the electrokinetic charge density

$$g \equiv \frac{F^2}{RT}c(P_1 + P_2 - 2\theta) \tag{36}$$

is the membrane electric conductivity at zero transmembrane volume flow.

For capillary models, the coefficients in Eqs. (30)–(36) are defined by

$$P_i \equiv \gamma\left[D_i\Gamma_i + RTc\widehat{F}[1]\left(\frac{\Gamma_i\widehat{F}[\Gamma_i]}{\widehat{F}[1]} - \tau_i^2\right)\right] \tag{37}$$

$$\theta \equiv RT\gamma cF[1]\cdot\left(\frac{\Gamma_1\widehat{F}[\Gamma_2]}{\widehat{F}[1]} - \tau_1\tau_2\right) \tag{38}$$

$$\tau_i \equiv \frac{\Gamma_i\widehat{F}[1]}{\widehat{F}[1]} \tag{39}$$

D_i are the ion diffusion coefficients, Γ_i are the coefficients of ion partitioning between a given point inside the pore and virtual solution, the brackets, , mean integration over the pore cross-section and scaling on its area, γ is the membrane porosity, τ_i are the ion transmission coefficients quantifying the extent to which ions are convectively entrained by the volume flow.[1] In principle, these coefficients can be affected by steric hindrance [40] but this is not significant in nanopores whose size is much larger than the ion size (the focus of this study). Based on the same considerations, we also neglect the effect of steric hindrance on the ion diffusion and consider ion diffusion coefficients in nanopores constant and equal to those in bulk electrolyte solution.

The linear functional operator $\widehat{F}[]$ featuring in Eqs. (37)–(39) gives solution(fluid velocity, $\vec{v}$) to this equation

$$\eta\nabla^2\vec{v} = -\vec{f} \tag{40}$$

where $\vec{f}$ is an arbitrary function of coordinate inside the pore. For long straight capillaries away from their edges, only one velocity component (along the capillary) is non-zero. In cylindrical capillaries, this component depends only on the radial position, r. In the case of solvent, $\Gamma_i = 1$, and for $\widehat{F}[1]$ we recover the well-known parabolic Hagen-Poiseuille velocity profile

$$\widehat{F}[1] = \frac{1}{4\eta}\left(r_p^2 - r^2\right) \tag{41}$$

$$\widehat{F}[1] \equiv \frac{r_p^2}{8\eta} \tag{42}$$

$$\chi \equiv \gamma\widehat{F}[1] \tag{43}$$

where η is the solution viscosity. $\widehat{F}[\Gamma_i]$ can be understood as an "iono-osmotic" fluid-velocity profile. The ion partitioning coefficients will be calculated by using non-linearized Poisson-Boltzmann equation (as described in Ref. [39]) with the surface-charge density as fitting parameter.

3. Experimental

The scheme of membrane cell is shown in Fig. 3. The active membrane diameter was 1.2 cm; the volume of half-cell was ca. 5.5 mL. The pressure was created by moving a bottle with the solution (1 mM or 2 mM KCl, p.a. (POCh Gliwice), demineralized water (<2 μS/cm, laboratory demineralizer Hydrolab)) connected to one of the cell compartments on a given height above the cell (above the valve v.3). Ag/AgCl electrodes were used; they were connected to a multi-meter (Unigor 380 with the memory mem 232). The sampling rate was 0.5 s. After mounting a membrane to the cell, the compartments were filled by opening the valves v.1, v.2 and v.3. After filling the compartments, the valves v.1 were closed, the valves v.3 were in a position connecting the compartments with the environment – no applied pressure to the membrane; the valves v.2 played only an auxiliary role in filling,

[1] Importantly, the ion convective flux in the pore is scaled on the ion concentration in the so-called virtual solution.

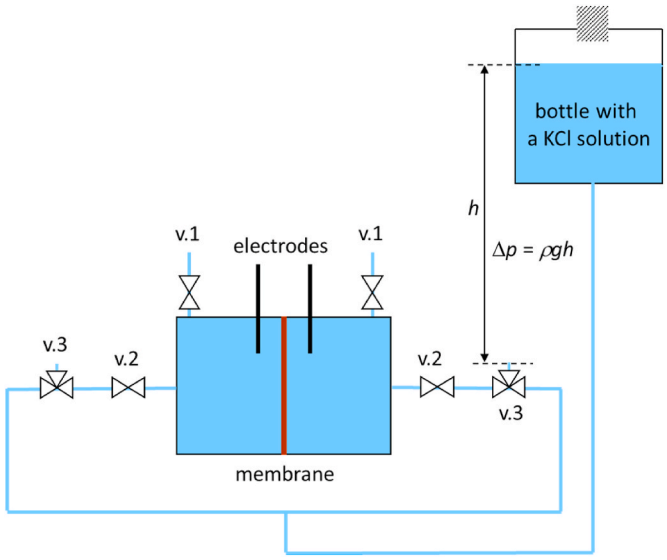

Fig. 3. Scheme of the test cell for the measurements of pressure-induced potential; the applied pressure, Δp, was calculated from the height of the solution level in the bottle above the v.3 outlet being in the half-cell-environment position; on the opposite side, v.3 is in the position half-cell-bottle.

emptying the cell. Then the data acquisition was started. After ca. 7 min the pressure was applied to one side of membrane by turning the valve v.3 of that compartment into the position connecting it with the bottle. The pressure was applied for ca. 30 s and then the valve v.3 was turned into the previous position (no pressure). This sequence was repeated at least three times. Then the same procedure was repeated for the pressure applied to the other membrane side; after that the data acquisition was stopped. The same was repeated for other pressures (ca. 2, 4, 7 and 10 kPa; in the calculations the exact values of pressure were used).

The temperature was 22–23 °C, solution pH5.2. This relatively low pH value occurred for solutions equilibrated with the ambient atmosphere for sufficiently long time. In preliminary measurements, we noticed that pH value of freshly-prepared solutions drifted, which impaired reproducibility of the measurements. Effectively, our working solutions were buffered by CO_2 dissolved from the atmosphere. Table 1 shows the properties of laboratory-made membranes used in this study. Their fabrication procedures are described in detail in the ECI of ref. [39].

4. Results and discussion

Fig. 4 shows a typical series of repeated measurements.

Due to the absence of stirring, eventual steady state (controlled by

Table 1
Properties of the membranes.

membrane	material	thickness (μm)	pore density (m^{-2})	pore diameter (nm)[a])	angle distribution[b])
1819	PET	10	$8{\cdot}10^{13}$	25	±30°
1811-II	PET	10	$5{\cdot}10^{13}$	35	±30°

*) PET = polyethylene terephthalate.
[a] determined from hydraulic permeability to pure water (see below).
[b] To avoid pore overlaps along the whole membrane thickness, irradiation is performed in such a way that the pores are not strictly perpendicular to the membrane surface (so the overlaps occur only punctually along the pore length), and the corresponding angle is evenly distributed within the indicated range. As described in Ref. [39], this makes the pores on average about 5% longer than the membrane thickness, which was accounted for in the interpretation.

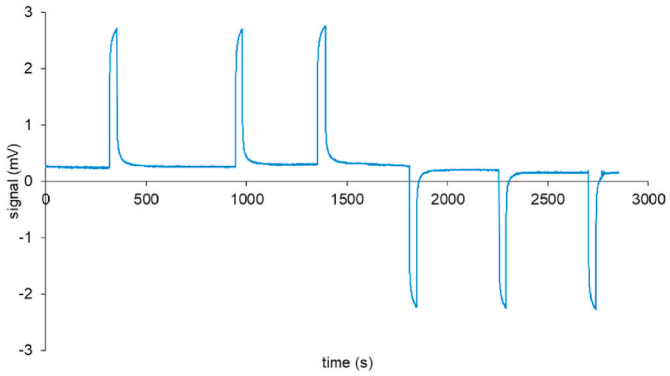

Fig. 4. An example of "raw" experimental data: $\Delta p = 7.1\ kPa$, membrane pore size 35 nm, 2 mM KCl solution.

natural convection) would be poorly defined, so we deliberately did not attempt to attain it and used only initial parts of the time dependencies. Each time, pressure difference was applied for about 30 s only. Owing to the short pressure application, the cumulative concentration changes were relatively small, so the system could easily return to equilibrium during the relatively long relaxation periods at zero pressure difference. This is confirmed by the signal reaching prolonged periods of constant values between the pressure-induced runs.

Pressure could be applied from either side of the membrane, and this was used to verify the independence of response from the membrane orientation: there was no statistically significant dependence which confirms the membrane monolayer structure. Some non-zero signal at zero pressure difference occurred due to potential of asymmetry of the electrodes. As one can see from Fig. 4, this potential slightly and slowly drifted with time. This drift was negligible at the time scale of the relatively short pressure-induced runs, so the signal was averaged over 10 s preceding each pressure application, and the corresponding value was subtracted from the measured signal to obtain genuine pressure-induced potential. The resulting data were averaged over 6–8 repeated measurements performed for each pressure. Fig. 5 shows the results plotted vs square root of time. Over the time of the measurements, the signal increases about two times compared to the initial value. Therefore, neglecting these phenomena and just identifying pressure-induced potential with streaming potential would give rise to considerable errors in interpretation.

One can see that (apart from the first data points taken immediately after the pressure application[2]) an excellent agreement between the model and experiment could be achieved. For not obscuring this quality, the graphs do not show error bars but average relative standard deviations are indicated in the legends and reveal a good to excellent reproducibility. Additionally, the ESI (Fig. S2) shows relative deviations of all data points from the theoretical fits. Apart from the first data points, the deviations never exceed 2%, and their overwhelming majority is well below 0.5%. Moreover, the graphs demonstrate that the deviations are evenly scattered around zero, which indicates that the functional form of the fitting function is correct.

Fig. 5 shows that both initial slopes and streaming potentials (extrapolated values at zero time) increase with applied pressure. Fig. 6 confirms this and additionally demonstrates that these increases are linear as they should be according to the model. All the R^2 values are above 0.996 (most are >0.999) and the offsets of extrapolations to zero pressure are <3% of the maximum values. The standard deviations shown in Fig. 6 were estimated as follows. For each individual run we determined the initial slope and signal extrapolated to zero time. These data for each pressure were averaged and standard deviations were obtained.

4.1. Interpretation within the scope of space-charge model

Having confirmed the applicability of the linear salt-transport model, now the slopes of linear dependencies shown in Fig. 6 will be interpreted within the scope of space-charge model.

Fig. 7 illustrates our interpretation approach. Fig. 7a) shows data for the slope of linear dependence on pressure of the initial slope of time dependencies on square root of time (shown in Fig. 6a)). According to Eq (29), this is equal to $\frac{RT}{F}\frac{8}{\sqrt{\pi}}\frac{\chi_*}{\sqrt{DL}}\sigma_s\Delta t_+$. The membrane hydraulic permeance χ_*/L was estimated using the results of independent measurements of pressure-driven pure-water volume flow as described in Ref. [39]. It was assumed that this permeance was not affected by the so-called electro-viscosity (quantified by the denominator in Eq (34)) because in very dilute solutions, the surface-charge density (controlling the phenomenon magnitude in very dilute solutions) tends to zero. From the hydraulic permeance and known membrane thickness (corrected for the pore non-perpendicularity, see Ref. [39]) and pore density, using Hagen-Poiseuille equation, we determined the membrane pore sizes (shown in Table 1). At the same time, in the theoretical calculations of the initial slope, the electroviscosity correction (given by Eq (34)) was accounted for. The bulk salt-diffusion coefficient, D, is known from literature, the membrane thickness is known, too. Thus, with a known pore size, one can calculate the initial slope of dependence on square-root of time theoretically (by using Eqs ((30), (31), (34), (37)–(39)) as a function of surface-charge density (blue and orange solid lines in Fig. 7a)) and compare it with the experimental value (indicated by the horizontal dashed line). The same can be done for the streaming-potential coefficient (obtainable directly from the slopes of linear dependencies in Fig. 6b).

The blue lines in Fig. 7 were calculated using the "classical" version of space-charge model postulating a smooth and impermeable pore surface. Projection on the horizontal axis of the intersect of blue solid line and the dashed line gives the corresponding value of negative surface-charge density ($-3.4\ mC/m^2$). The same procedure applied to the streaming-potential coefficient (Fig. 7b)) produces the value of only about $-1.1\ mC/m^2$. Qualitatively similar discrepancies occur for the other combinations of membrane pore size and KCl concentrations used in this study (see Fig. S3 in the ESI). Though both values are always of the same order of magnitude, the difference is significant (about 3 times) and can hardly be ascribed to experimental errors given the excellent reproducibility of our experimental data and high fidelity of their interpretation in terms of membrane transport properties.

The initial-slope data depend on the membrane porosity and thickness whereas streaming-potential data are independent of them: a close inspections of Eqs (33), (37), (38) and (43) shows that the porosity in the definition of streaming-potential coefficient cancels out and the membrane thickness does not feature in it, at all. Technically, we could not measure the membrane hydraulic permeability directly in the test cell used in this study, and membrane samples could not be reused after measurements in a separate test cell due to a damage by its O-ring. Therefore, information on the hydraulic permeabilities is burdened with some uncertainty primarily related to variability in the track density (±10%). However, assuming that the correct value of surface-charge density corresponds to the streaming-potential coefficient, we would need to speculate that the membrane hydraulic permeability actually was about 3 times larger (this would shift the blue curve up in Fig. 7a) until it crosses the horizontal dashed line at the negative surface-charge density of ca.-1.1 mC/m^2). This is far beyond the uncertainty of ±10%. Besides, such a dramatic increase in membrane porosity over thickness ratio would cause a strong decrease in the characteristic relaxation time (see Eq (14) showing this time to be inversely proportional to the square

[2] These deviations of the first data points are probably due to the fact that the *trans*-membrane pressure difference could not be established instantaneously but took some finite time comparable to the time step of our measurements (0.5 s).

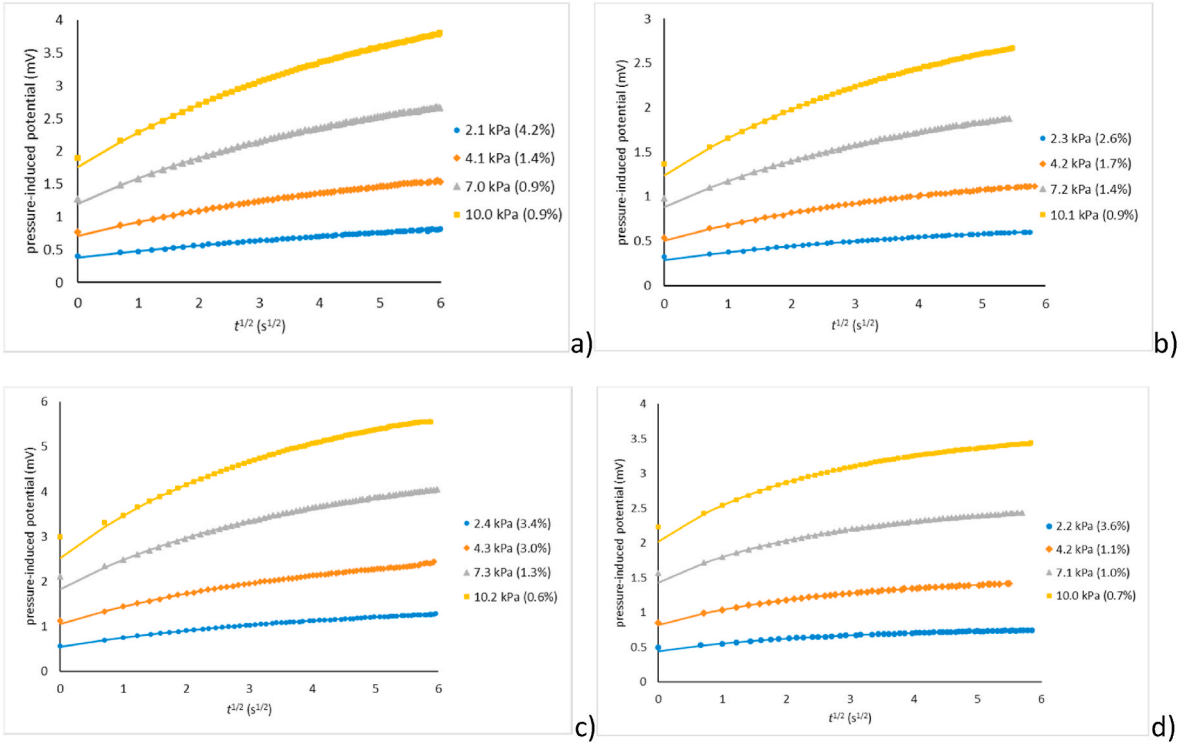

Fig. 5. Pressure-induced potential (symbols) and its theoretical fits (lines): pore size: 25 nm (a,b), 35 nm (c,d); KCl concentration: 1 mM (a,c), 2 mM (b,d); the legends indicate the applied pressures and average relative standard deviations of the data from the model (numbers in parenthesis). The theoretical curves were calculated by using Eqs ((9), (14), (24) and (28) and the experimental values of parameters listed in Table 2.

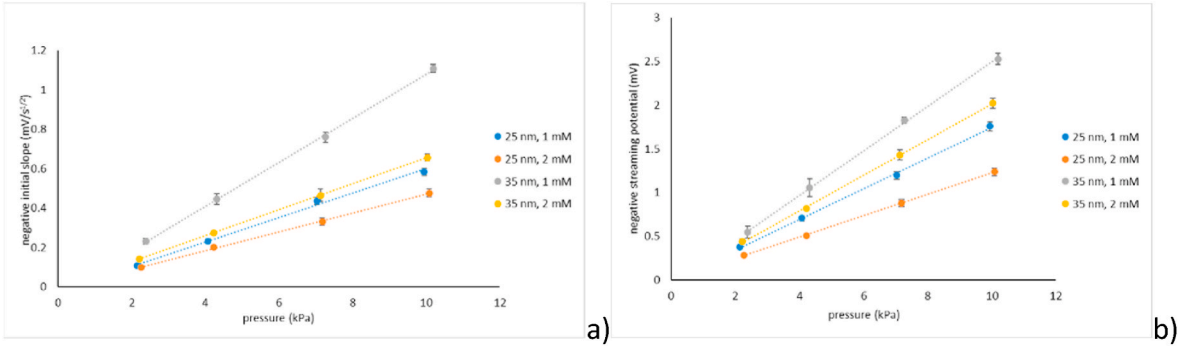

Fig. 6. Pressure dependencies of initial slope (a) and streaming potential (b).

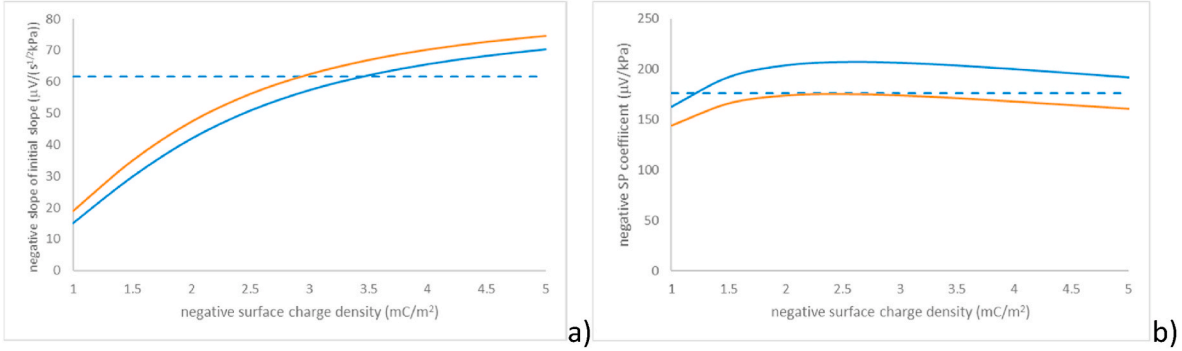

Fig. 7. Theoretical dependencies of slope of initial slope (a) and streaming-potential coefficient (b) on surface-charge density and their comparison with experimental values (horizontal dashed lines): 25 nm membrane, 1 mM KCl solution; the blue lines were calculated assuming a smooth non-porous nanopore surface, the orange lines were obtained postulating the existence of a "gel" layer on the pore surface. (For interpretation of the references to colour in this figure legend, the reader is referred to the Web version of this article.)

of this ratio). Below, we will see that experimental relaxation times were actually somewhat longer than expected and not much shorter as it would occur if the "high-porosity" hypothesis applied.

An alternative explanation of the mismatch between the "initial-slope" and "streaming-potential" surface-charge densities is based on the hypothesis of the so-called "gel" layers around pores of nanoporous grades of track-etched membranes [41–44]. Reportedly, they occur because of relatively short etching, so not all the polymer damaged by secondary electrons arising during heavy-ion passage is etched out. This remaining damaged polymer contains dissociating groups, can swell and allow for some ion permeation. At the same time, its hydraulic permeability is probably negligibly low. We consider it equal to zero, so the ion transmission coefficients are not directly affected because they are controlled by ion partitioning averaged with the flow velocity profile (see Eq (39)). Of course, there may be indirect impact via dependence of ion-partitioning coefficients on the surface-charge distribution within a layer of finite thickness but we disregard this. Further, we assume that coions are completely excluded from the gel layer, because "pores" in it are very small and very well overlapped by diffuse parts of EDLs. Thus, effectively we consider the gel layer as an additional "channel" of unipolar counterion conductance put in parallel to the pore. This gives rise to an increase in the counterion permeability featuring in Eqs. (30)–(33) without affecting any other coefficients (for example, within the scope of our model the coefficient of "mutual electro-diffusion", θ, is controlled by liquid flows and, thus, is not affected).

The orange curves in Fig. 7 were calculated considering the effect of such additional counterion conductance. By adjusting its magnitude, streaming-potential coefficient can be shifted down. At the same time, the initial-slope coefficient somewhat increases (primarily, due to the increase of transport number of counterions in the membrane but also because of some related increase of salt-reflection coefficient) but this is less pronounced. Overall, from Fig. 7 (and Fig. S3 in the ESI) one can see that introduction of additional counterion conductance affords reconciliation of the surface-charge densities corresponding to the initial-slope and streaming-potential coefficients. Table 2 lists the relative increases in the counterion conductance due to the hypothetical gel layer needed to achieve this agreement. As one can see, the corrections are moderate. By the order of magnitude, they correspond to the ratio of gel-layer cross-section to that of the pore.

From the experimental data, we could also determine the characteristic relaxation times. Given that their finite values manifest themselves in deviations of plots in Fig. 5 from linearity (and these deviations are not very much pronounced), the accuracy of these estimates is not very high. By using the surface-charge density fitted to the initial-slope coefficient (with and without the gel-layer correction) we could calculate theoretical values of characteristic relaxation time (using (Eqs ((14), (32), (37) and (38)). Comparison of experimental and theoretical values reveals that agreement is actually better without the gel-layer correction and is very good (within experimental error) with the exception of 35-nm membrane in 1 mM solution where the difference is also not very large (ca.15%). Thus, the gel-layer hypothesis helps reconcile initial-slope and streaming-potential coefficients but makes agreement with the characteristic relaxation times worse. One should also keep in mind that the way we included gel layers in our model is not very sophisticated. However, we don't have enough experimental data to provide input for more elaborate versions. As mentioned above, one of the principal uncertainties in the interpretation is related to sample-to-sample variability of membrane porosity (track density). Therefore, in future studies we plan to develop equipment making possible measurements of hydraulic permeability and transient pressure-induced potential for the same membrane sample. Besides, parallel measurements of osmotic pressure, salt diffusion [39] (also for the same membrane sample) as well as, ideally, membrane potential could also be very useful.

Similarly to several previous studies [20,35,39], we observe considerable increase of surface-charge density in PET track-etched membranes with the salt concentration. This has been explained by stronger dissociation of weakly-acidic surface groups at higher concentrations where electrostatic adsorption of H^+ ions is reduced.

Finally, with the fitted values of surface-charge densities, we can make a posteriori estimates of Péclet numbers in our measurements. The ESI shows that at the maximum pressure of approximately 10 kPa they were about 0.1–0.12 in the 25-nm pore membrane and around 0.14–0.17 in the 35-nm pore membrane (depending on the salt concentration and assumption of gel layer). This confirms that the Péclet numbers were small and the linear approximation in them was applicable, which is in agreement with the excellent linearity of the plots in Fig. 6.

4.2. Comparison with previous work

Ref. [39] studied the same track-etched membrane as one of the used in this work (25 nm) but employing different experimental methods (parallel measurements of osmotic pressure and salt diffusion). For the average KCl concentration of 1.5 mM, this study estimated the surface-charge density of −5.7 mC/m^2, which is close to the values interpolated to this concentration from Table 2 (−4.6 mC/m^2 or -3.8 mC/m^2 without or with the gel-layer correction). They are somewhat lower than in Ref. [39] but this may be due to a lower solution pH in the present study. As mentioned above, surface charge in these membranes arises due to dissociation of weakly-acidic groups and, thus, can noticeably decrease with decreasing pH just within the pH5-6 range. In Ref. [35], surface-charge density of a similar (commercial) PETP track-etched membrane was estimated from measurements of membrane potential after current switch-off. For a comparable value of KCl concentration (1.25 mM, pH5.6) the surface-charge density was estimated at ca.-4 mC/m^2, which is very close to the values obtained in the present study. The same commercial PET track-etched membrane was also studied in Ref. [20] using transient filtration potential after pressure switch-off. From these measurements, in 2.5 mM KCl solution of pH5.7 the surface-charge density was estimated at ca.-14 mC/m^2, which is essentially larger than in the present work. The surface-charge density in

Table 2
Parameters estimated from experimental data and space-charge model.

membrane/ solution	initial-slope coeff. (μV/s$^{1/2}$*kPa)	SP coeff. (μV/ kPa)	$\sqrt{t_{rel}}$ (exp.) (s$^{1/2}$)	surface-charge density (mC/m^2)	surface-charge density (corr.) (mC/m^2)	$\sqrt{t_{rel}}$ (th.) (s$^{1/2}$)	$\sqrt{t_{rel}}$ (th. corr.) (s$^{1/2}$)	gel-layer corr.
25 nm, 1 mM	−62	−176	8.0 ± 0.5	−3.4	−2.9	7.8	6.8	18%
25 nm, 2 mM	−48	−123	6.6 ± 0.2	−5.7	−4.7	6.5	5.7	38%
35 nm, 1 mM	−112	−254	5.7 ± 0.4	−3.6	−2.8	4.8	4.1	41%
35 nm, 2 mM	−66	−203	3.5 ± 0.1	−5.1	−4.1	3.7	3.3	36%

corr. = with the gel-layer correction.

Ref. [20] was fitted to streaming-potential coefficient. As we have seen above (see Fig. 7 and Fig. S3), one value of streaming-potential coefficient can correspond to two essentially different values of surface-charge density. The high surface-charge density in Ref. [20] likely corresponded to the second intercept point. This is indirectly confirmed by the fact that the experimental values of membrane potential determined in Ref. [20] were considerably overestimated by the model using the value of -14 mC/m^2.

4.3. Applicability of the methodology to composite/asymmetric membranes

This study deals with monolayer membranes. It is interesting to consider briefly to what extent its methodology can be extended to more practical composite and/or asymmetric membranes. Expectedly, the situation in this case is more complicated. Firstly, support layers of such membranes have been demonstrated to make noticeable (if not principal) contribution to streaming potential [45]. This is a problem because the primary goal of characterization is obtaining information on the properties of barrier (active) layers. Remarkably, support layers do not directly contribute to concentration changes, so the time-dependent component of filtration potential is affected only indirectly which, in principle, can be taken into account. Secondly, the presence of support layers on one side of the actual solute-rejecting membrane (active layer) makes non-stationary concentration profiles deviate from the simple antisymmetric pattern shown in Fig. 1. The profiles (and electrical response) become dependent on the porosity and effective diffusion coefficient of solute within the support layer. These properties are usually unknown, so in the interpretation they have to be considered fitting parameters. Adding two more adjustable parameters would probably make unambiguous interpretation impossible. Therefore, additional measurements would be needed. Transient membrane potential in a composite membranes was studied by pressure switch-off method [46]. In this case, additional input was obtained from the measurements of steady-state salt rejection. However, in the simple setup used in this study, determination of steady-state salt rejection is not possible. In summary, for characterization of composite/asymmetric membranes via measurement of time-resolved transmembrane potential, the pressure switch-off method should rather be used.

5. Conclusions

With nanoporous membranes featuring noticeable salt rejection, determination of genuine streaming potential is non-trivial and requires time-resolved measurements. A new approach to the interpretation of such measurements developed and tested experimentally in this study makes possible parallel determination of several membrane transport properties, namely, the product of salt-reflection coefficient and difference of ion transport numbers between the membrane and solution, streaming-potential coefficient and membrane diffusion permeance to salt. Previously, only streaming-potential coefficient was determined from time-resolved measurements. In nanoporous membranes, this coefficient is a non-monotone function of surface-charge density, which makes difficult unambiguous determination of the latter. On the contrary, the other properties determined in this study are monotone functions of surface-charge density.

We used a simple experimental setup that (due to the use of small pressure differences) can be easily implemented. Besides, the “linear” experimental conditions made applicable a simple (but novel) theoretical model for the interpretation of time transients after pressure application. Its detailed comparison with experimental data revealed excellent applicability, relative deviations of model from experimental data being mostly below 0.5%.

This approach has been validated via characterization of two nanoporous track-etched membranes (with the pore sizes of 25 nm and 35 nm) in KCl solutions of two different concentrations (1 mM and 2 mM). The transport properties “extracted” from experimental data were used as input of full (numerical) version of space-charge model. This made possible determination of surface-charge density as well as some properties of hypothetical gel layers reportedly surrounding pores of nanoporous grades of track-etched membranes.

These results are important for optimization of applications of nanoporous charged membranes in ion separations and electrokinetic energy conversion.

Author contributions

Pavel Apel: membrane fabrication and characterization, data interpretation, manuscript editing, Stanisław Koter: experimental methodology, building experimental setup, experimentation, data interpretation, Andriy Yaroshchuk: conceptualization, theoretical analysis, data interpretation, writing and editing.

Declaration of competing interest

The authors declare that they have no known competing financial interests or personal relationships that could have appeared to influence the work reported in this paper.

Acknowledgements

A.Y. acknowledges funding from the European Union through Project H2020-FETOPEN-2018-2019-2020-01-964524 “Energy harvesting via wetting/drying cycles with nanoporous electrodes (EHAWEDRY)”. S.K. thanks for the funds for fundamental research from Nicolaus Copernicus University in Torun, Poland (Faculty of Chemistry – “Membranes and membrane separation processes - fundamental and applied research”).

Appendix A. Supplementary data

Supplementary data to this article can be found online at https://doi.org/10.1016/j.memsci.2022.120556.

Nomenclature

$A(\omega)$ $(-)$ frequency-dependent coefficient
c (mol/m^3) salt concentration
c_0 (mol/m^3) initial salt concentration
D (m^2/s) salt diffusion coefficient in solution
D_i (m^2/s) ion diffusion coefficient
D_m (m^2/s) salt diffusion coefficient in membrane pores
F $(A\cdot s/mol)$ Faraday constant
$\widehat{F}[]$ $(m^2/Pa\cdot s)$ linear operator

$g\ (S/m)$ membrane electric conductivity
$H(\tau)\ (-)$ unit-step function
$H(\omega)\ (-)$ Fourier-transform of unit-step function
$i\ (-)$ imaginary unit
$J\ (mol/m^2 \cdot s)$ salt flux
$J_m\ (mol/m^2 \cdot s)$ *trans*-membrane salt flux
$J_v\ (m/s)$ *trans*-membrane volume flux
$J_{v0}\ (m/s)$ constant *trans*-membrane volume after pressure application
$L\ (m)$ membrane thickness
$p\ (Pa)$ hydrostatic pressure
$P_m\ (m/s)$ salt diffusion permeance of membrane
$P_i\ (m^2/s)$ membrane permeability to ion "i"
$P_s\ (m^2/s)$ membrane diffusion permeability to salt
$Pe\ (-)$ Péclet number
$Pe_0\ (-)$ constant Péclet number after pressure application
$R\ (J/mol)$ universal gas constant
$r\ (m)$ radial cylindrical coordinate
$r_p\ (m)$ cylindrical-pore radius
$s\ (-)$ dimensionless deviation of salt concentration from initial value
$T\ (K)$ absolute temperature
$t\ (s)$ time
$t_{ch}\ (s)$ characteristic relaxation time
$t_i\ (-)$ transport number of ion "i"
$t_+^{(m)}\ (-)$ cation transport number in membrane
$t_+^{(b)}\ (-)$ cation transport number in solution
$\vec{v}\ (m/s)$ fluid velocity
$x\ (m)$ coordinate

Greek symbols
$\alpha\ (V \cdot m/Pa)$ streaming-potential coefficient
$\gamma\ (-)$ membrane porosity
$\delta\ (m)$ thickness of stagnant layer
$\Gamma_i\ (-)$ local partitioning coefficient of ion "i" inside membrane pore
$\eta\ (Pa \cdot s)$ dynamic viscosity
$\xi\ (-)$ dimensionless coordinate
$\theta\ (m/s)$ coefficient of mutual electro-diffusion
$\chi\ (m^2/Pa \cdot s)$ membrane hydraulic permeability at zero voltage difference
$\chi_*\ (m^2/Pa \cdot s)$ membrane hydraulic permeability at zero current
$\rho_{ek}\ (A \cdot s/m^3)$ electrokinetic charge density
$\sigma_s\ (-)$ salt reflection coefficient
$\tau\ (-)$ dimensionless time
$\tau_i\ (-)$ transmission coefficient of ion "i"
$\omega\ (-)$ dimensionless circular frequency

References

[1] C. Tang, A. Yaroshchuk, M.L. Bruening, Flow through negatively charged, nanoporous membranes separates Li+and K+due to induced electromigration, Chem. Commun. 56 (2020) 10954–10957, https://doi.org/10.1039/d0cc03143g.
[2] A.E. Yaroshchuk, Osmosis and reverse osmosis in fine-porous charged diaphragms and membranes, Adv. Colloid Interface Sci. 60 (1995) 1–93.
[3] C. Bardot, E. Gaubert, A. Yaroshchuk, Unusual mutual influence of electrolytes during pressure-driven transport of their mixtures across charged porous membranes, J. Membr. Sci. 103 (1995) 11–17.
[4] A. Bentien, T. Okada, S. Kjelstrup, Evaluation of nanoporous polymer membranes for electrokinetic energy conversion in power applications, J. Phys. Chem. C 117 (2013) 1582–1588, https://doi.org/10.1021/jp308957q.
[5] S. Haldrup, J. Catalano, M.R. Hansen, M. Wagner, G.V. Jensen, J.S. Pedersen, A. Bentien, High electrokinetic energy conversion efficiency in charged nanoporous nitrocellulose/sulfonated polystyrene membranes, Nano Lett. 15 (2015) 1158–1165, https://doi.org/10.1021/nl5042287.
[6] S. Haldrup, J. Catalano, M. Hinge, G.V. Jensen, J.S. Pedersen, A. Bentien, Tailoring membrane nanostructure and charge density for high electrokinetic energy conversion efficiency, ACS Nano 10 (2016) 2415–2423, https://doi.org/10.1021/acsnano.5b07229.
[7] A. Szymczyk, P. Fievet, J.C. Reggiani, J. Pagetti, Electrokinetic characterization of mixed alumina-titania-silica MF membranes by streaming potential measurements, Desalination 115 (1998) 129–134. http://www.sciencedirect.com/science/article/pii/S0011916498000320.
[8] A. Christoulaki, D. Lairez, E. Dubois, N. Jouault, Probing polyelectrolyte adsorption in charged nanochannels by streaming potential measurements, ACS Macro Lett. 9 (2020) 794–798, https://doi.org/10.1021/ACSMACROLETT.0C00172.
[9] P. Déjardin, E.N. Vasina, V.V. Berezkin, V.D. Sobolev, V.I. Volkov, Streaming potential in cylindrical pores of poly(ethylene terephthalate) track-etched membranes: variation of apparent zeta potential with pore radius, Langmuir 21 (2005) 4680–4685. http://www.ncbi.nlm.nih.gov/pubmed/16032889.
[10] K.J. Kim, A.G. Fane, M. Nyström, A. Pihlajamaki, Chemical and electrical characterization of virgin and protein-fouled polycarbonate track-etched membranes by FTIR and streaming-potential measurements, J. Membr. Sci. 134 (1997) 199–208, https://doi.org/10.1016/S0376-7388(97)00113-0.
[11] L. Ricq, J. Pagetti, Inorganic membrane selectivity to ions in relation with streaming potential, J. Membr. Sci. 155 (1999) 9–18, https://doi.org/10.1016/S0376-7388(98)00277-4.
[12] S. Condom, S. Chemlal, W. Chu, M. Persin, A. Larbot, Correlation between selectivity and surface charge in cobalt spinel ultrafiltration membrane, Separ. Purif. Technol. 25 (2001) 545–548, https://doi.org/10.1016/S1383-5866(01)00125-3.
[13] S. Datta, A.T. Conlisk, D.M. Kanani, A.L. Zydney, W.H. Fissell, S. Roy, Characterizing the surface charge of synthetic nanomembranes by the streaming potential method, J. Colloid Interface Sci. 348 (2010) 85–95, https://doi.org/10.1016/j.jcis.2010.04.017.
[14] J.I.I. Calvo, A. Hernández, P. Prádanos, F. Tejerina, Charge adsorption and zeta potential in cyclopore membranes, J. Colloid Interface Sci. 181 (1996) 399–412, https://doi.org/10.1006/jcis.1996.0397.

[15] I.H. Huisman, P. Prádanos, A. Hernández, Electrokinetic characterisation of ultrafiltration membranes by streaming potential , electroviscous effect , and salt retention, J. Membr. Sci. 178 (2000) 55–64, https://doi.org/10.1016/S0376-7388(00)00479-8.
[16] M. Sbaï, P. Fievet, A. Szymczyk, B. Aoubiza, A. Vidonne, A. Foissy, Streaming potential, electroviscous effect, pore conductivity and membrane potential for the determination of the surface potential of a ceramic ultrafiltration membrane, J. Membr. Sci. 215 (2003) 1–9, https://doi.org/10.1016/S0376-7388(02)00553-7.
[17] S. Condom, S. Chemlal, A. Larbot, M. Persin, Behaviour of a cobalt spinel ultrafiltration membrane during salt filtration with different ionic strengths, J. Membr. Sci. 268 (2006) 175–180, https://doi.org/10.1016/j.memsci.2005.06.006.
[18] J. Benavente, G. Jonsson, Electrokinetic characterization of composite membranes : estimation of different electrical contributions in pressure induced potential measured across reverse osmosis membranes, J. Membr. Sci. 172 (2000) 189–197.
[19] Y. Zhang, T. Xu, An experimental investigation of streaming potentials through homogeneous ion-exchange membranes, Desalination 190 (2006) 256–266, https://doi.org/10.1016/j.desal.2005.09.006.
[20] A. Yaroshchuk, Y. Boiko, A. Makovetskiy, Ion-rejection, electrokinetic and electrochemical properties of a nanoporous track-etched membrane and their interpretation by means of space charge model, Langmuir 25 (2009) 9605–9614, https://doi.org/10.1021/la900737q.
[21] M.A. Islam, N.D. Nikolov, J.D. Nikolova, An electrical model for the relaxation of streaming potential across a charged membrane, J. Membr. Sci. 84 (1993) 29–36, https://doi.org/10.1016/0376-7388(93)85048-2.
[22] J.A. Ibañez, J. Forte, A. Hernandez, F. Tejerina, Streaming potential and phenomenological coefficients in nuclepore membranes, J. Membr. Sci. 36 (1988) 45–54, https://doi.org/10.1016/0376-7388(88)80005-X.
[23] T. Okada, S. Kjelstrup Ratkje, H. Hanche-Olsen, Water transport in cation exchange membranes, J. Membr. Sci. 66 (1992) 179–192, https://doi.org/10.1016/0376-7388(92)87008-L.
[24] E. Brendler, S. Kjelstrup Ratkje, H.G. Hertz, Streaming potentials of Nucleopore membranes by the electric work method, Electrochim, Acta 41 (1996) 169–176.
[25] F.A. Morrison, J.F. Osterle, Electrokinetic energy conversion in ultrafine capillaries, J. Chem. Phys. 43 (1965) 2111, https://doi.org/10.1063/1.1697081.
[26] R.J. Gross, J.F. Osterle, Membrane transport characteristics of ultrafine capillaries, J. Chem. Phys. 49 (1968) 228–234, https://doi.org/10.1063/1.1669814.
[27] A. Szymczyk, B. Aoubiza, P. Fievet, J. Pagetti, Electrokinetic phenomena in homogeneous cylindrical pores, J. Colloid Interface Sci. 216 (1999) 285–296, https://doi.org/10.1006/jcis.1999.6321.
[28] A. Szymczyk, P. Fievet, B. Aoubiza, C. Simon, J. Pagetti, An application of the space charge model to the electrolyte conductivity inside a charged microporous membrane, J. Membr. Sci. 161 (1999) 275–285, https://doi.org/10.1016/S0376-7388(99)00118-0.
[29] P. Fievet, B. Aoubiza, A. Szymczyk, J. Pagetti, Membrane potential in charged porous membranes, J. Membr. Sci. 160 (1999) 267–275, https://doi.org/10.1016/S0376-7388(99)00090-3.
[30] P. Fievet, A. Szymczyk, B. Aoubiza, J. Pagetti, Evaluation of three methods for the characterisation of the membrane-solution interface: streaming potential, membrane potential and electrolyte conductivity inside pores, J. Membr. Sci. 168 (2000) 87–100, https://doi.org/10.1016/S0376-7388(99)00302-6.
[31] P.B. Peters, R. van Roij, M.Z. Bazant, P.M. Biesheuvel, Analysis of electrolyte transport through charged nanopores, Phys. Rev. E. 93 (2016), 053108, https://doi.org/10.1103/PhysRevE.93.053108.
[32] A.E. Yaroshchuk, S.S. Dukhin, Phenomenological theory of reverse osmosis in macroscopically homogeneous membranes and its specification for the capillary space-charge model, J. Membr. Sci. 79 (1993), https://doi.org/10.1016/0376-7388(93)85113-B.
[33] C. Amatore, S. Szunerits, L. Thouin, J.-S. Warkocz, The real meaning of Nernst's steady diffusion layer concept under non-forced hydrodynamic conditions. A simple model based on Levich's seminal view of convection, J. Electroanal. Chem. 500 (2001) 62–70, https://doi.org/10.1016/S0022-0728(00)00378-8.
[34] J.K. Novev, R.G. Compton, Natural convection effects in electrochemical systems, Curr. Opin. Electrochem. 7 (2018) 118–129, https://doi.org/10.1016/j.coelec.2017.09.010.
[35] A. Yaroshchuk, O. Zhukova, M. Ulbricht, V. Ribitsch, Electrochemical and other transport properties of nanoporous track-etched membranes studied by the current switch-off technique, Langmuir 21 (2005) 6872–6882, https://doi.org/10.1021/la050499g.
[36] A. Yaroshchuk, Y. Boiko, A. Makovetskiy, Electrochemical perm-selectivity of active layers and diffusion permeability of supports of an asymmetric and a composite NF membrane studied by concentration-step method, Desalination 245 (2009) 374–387, https://doi.org/10.1016/j.desal.2009.02.001.
[37] A.E. Yaroshchuk, Negative rejection of ions in pressure-driven membrane processes, Adv. Colloid Interface Sci. 139 (2008) 150–173, https://doi.org/10.1016/j.cis.2008.01.004.
[38] A. Yaroshchuk, M.P. Bondarenko, Current-induced concentration polarization of nanoporous media: role of electroosmosis, Small 14 (2018), 1703723, https://doi.org/10.1002/SMLL.201703723.
[39] P. Apel, M. Bondarenko, Y. Yamauchi, A. Yaroshchuk, Osmotic pressure and diffusion of ions in charged nanopores, Langmuir 37 (2021) 14089–14095, https://doi.org/10.1021/ACS.LANGMUIR.1C02267/SUPPL_FILE/LA1C02267_SI_001.PDF.
[40] A. Yaroshchuk, M.L. Bruening, E. Zholkovskiy, Modelling nanofiltration of electrolyte solutions, Adv. Colloid Interface Sci. 268 (2019) 39–63, https://doi.org/10.1016/j.cis.2019.03.004.
[41] P. Apel, A. Schulz, R. Spohr, C. Trautmann, V. Vutsadakis, Track size and track structure in polymer irradiated by heavy ions, Nucl. Instrum. Methods Phys. Res. Sect. B Beam Interact. Mater. Atoms 146 (1998) 468–474, https://doi.org/10.1016/S0168-583X(98)00445-5.
[42] P. Déjardin, E.N. Vasina, V.V. Berezkin, V.D. Sobolev, V.I. Volkov, Streaming potential in cylindrical pores of poly(ethylene terephthalate) track-etched membranes: variation of apparent ζ potential with pore radius, Langmuir 21 (2005) 4680–4685, https://doi.org/10.1021/LA046913E.
[43] P.Y. Apel, I.V. Blonskaya, O.M. Ivanov, O.V. Kristavchuk, N.E. Lizunov, A. N. Nechaev, O.L. Orelovich, O.A. Polezhaeva, S.N. Dmitriev, Creation of ion-selective membranes from polyethylene terephthalate films irradiated with heavy ions: critical parameters of the process, Membr. Membr. Technol. 22 (2) (2020) 98–108, https://doi.org/10.1134/S251775162002002X, 2020.
[44] I.V. Blonskaya, O.V. Kristavchuk, A.N. Nechaev, O.L. Orelovich, O.A. Polezhaeva, P.Y. Apel, Observation of latent ion tracks in semicrystalline polymers by scanning electron microscopy, J. Appl. Polym. Sci. 138 (2021), 49869, https://doi.org/10.1002/APP.49869.
[45] A.E. Yaroshchuk, Y.P. Boiko, A.L. Makovetskiy, Filtration potential across membranes containing selective layers, Langmuir 18 (2002) 5154–5162, https://doi.org/10.1021/la025503s.
[46] A.E. Yaroshchuk, Y.P. Boiko, A.L. Makovetskiy, Some properties of electrolyte solutions in nanoconfinement revealed by the measurement of transient filtration potential after pressure switch off, Langmuir 21 (2005) 7680–7690, https://doi.org/10.1021/la050917h.